future pharmacology

MDPI

Article

Interaction of Microcolin Cyanobacterial Lipopeptides with Phosphatidylinositol Transfer Protein (PITP)—Molecular Docking Analysis

Christian Bailly [1,2,*] and Gérard Vergoten [3]

[1] Canther–Cancer Heterogeneity, Plasticity and Resistance to Therapies, CNRS, Inserm, UMR9020–UMR1277, University of Lille, Centre Hospitalier Universitaire de Lille, 59000 Lille, France
[2] Oncowitan, Scientific Consulting Office, 59290 Lille, France
[3] Lille Inflammation Research International Centerr, U1286-INFINITE-Inserm, Faculty of Pharmacy, University of Lille, ICPAL, 3 rue du Professeur Laguesse, 59000 Lille, France
* Correspondence: christian.bailly@univ-lille.fr

Abstract: Background/Objectives: Microcolins A–M are cytotoxic marine lipopeptides produced by the cyanobacterium *Moorena producens*, also known as *Lyngbya majuscula*. Recent studies have shown that two compounds in the series, microcolins B and H, can form covalent complexes with phosphatidylinositol transfer proteins α and β (PITPα/β) upon the reaction of their α,β-unsaturated ketone group with the thiol group of a key cysteine residue of PITP. These observations prompted us to compare the binding of all microcolins and a few related derivatives (VT01454 and (deoxy)majusculamide D) to PITP to delineate structure–binding relationships. **Methods**: A molecular docking analysis led to the identification of microcolin E as the potentially best PITPα binder in the series, followed by microcolins B and H and analog VT01454. The computational data agree well with the published experimental results. **Results:** The binding of microcolin H into a large cavity of PITPα positions its reactive electrophilic α,β-unsaturated ketone close to the thiol of Cys95, enabling the facile formation of a covalent C-S linkage. A similar bonding can occur with the Cys94 of PITPβ. Molecular models of microcolins bound to PITP were compared to identify structural elements chiefly implicated in the recognition process. **Conclusions**: This computational study provides guidance in the design of microcolin derivatives targeting PITPα/β considered targets for cancer and inflammatory pathologies.

Keywords: marine natural products; microcolin; molecular modeling; phosphatidylinositol transfer proteins; PITPα; PITPβ

Academic Editor: Giuseppe Floresta

Received: 16 February 2025
Revised: 10 March 2025
Accepted: 13 March 2025
Published: 17 March 2025

Citation: Bailly, C.; Vergoten, G. Interaction of Microcolin Cyanobacterial Lipopeptides with Phosphatidylinositol Transfer Protein (PITP)—Molecular Docking Analysis. *Future Pharmacol.* **2025**, *5*, 13. https://doi.org/10.3390/futurepharmacol5010013

1. Introduction

The tropical marine cyanobacterium *Moorena producens* JHB is a rich source of secondary metabolites with potential biomedical utility. This benthic filamentous cyanobacterium, previously known as *Lyngbya majuscula* (family Oscillatoriaceae), grows in marine and estuarine environments across the world. It has been observed in the Pacific Sea, the Caribbeans, the Gulf of Mexico, Singapore area, Venezuelan waters and many other places [1]. It is an invasive and toxic organism which can cause can severe irritations, papulovesicular eruptions and other dermatological affections [2]. Blooms of *M. producens* and their invasiveness are threats to the marine environment, and they are of great concern to the aquaculture and tourism industry [3,4].

Numerous bioactive metabolites have been isolated from this species, such as the products called hectochlorins, hectoramides, tiahuramides, lagunamides and jamaicamides [5–7].

Diverse products of medicinal interest have been characterized from *M. producens*, such as the antimalarial cyclic peptide kakeromamide B which can stimulate actin polymerization in cells [8], the antitumor lipopeptide kalkitoxin [9], the cytotoxin neo-aplysiatoxin A [10] and poisoning products lyngbyatoxins [11,12], to cite only a few examples. A recent chemical survey led to the identification of >230 natural products from 66 groups from *M. producens*, with 3 dominant groups: malyngamides, microcolins and dolastatins [4].

Microcolins represent one of the three main groups of cytotoxic lipopeptides isolated from this species with a series of 13 products—microcolins A to M (Figure 1)—endowed with cytotoxic properties [13]. The first two members in the series microcolins A and B were discovered more than 30 years ago and found to exhibit immunosuppressant and antiproliferative activities, acting as inhibitors of interleukin IL-2 production and modulators of the lymphocyte response [14–16]. They paved the way in the design of synthetic analogs with reinforced immunosuppressive properties [17] and in the design of chemical probes for elucidating their mechanism of action [18]. Microcolin A has been shown to target the early immature $CD4^+CD8^+$ T-cell subpopulation in thymocytes [16].

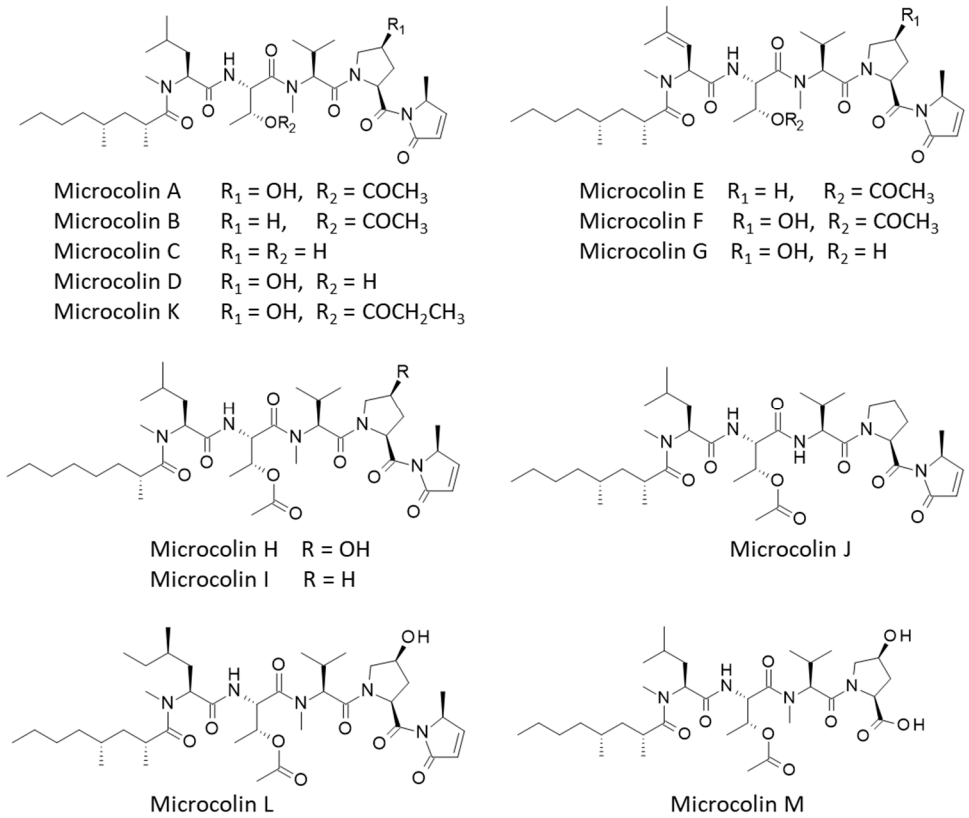

Figure 1. Structures of microcolins A–M.

The immune-suppressive action of microcolins was rarely investigated until the recent finding that microcolin B targeted phosphatidylinositol transfer proteins α and β (PITPα/β) [19]. PITPs are lipid-binding proteins which bind and transfer phosphatidylinositol and phosphatidylcholine from one membrane compartment to another. PITPα/β are ubiquitously expressed small (35 kDa) proteins with a single PITP domain [20–22]. It has been demonstrated that microcolin B and a synthetic structural analog VT01454 can bind directly to PITPβ via a covalent linkage to its Cys94 residue (Figure 1) [19].

The formation of a drug–PITP complex is responsible for the regulation of the Hippo pathway, a key signaling route playing a significant role in cell differentiation, proliferation and survival. It is frequently dysregulated in human cancers [23]. Microcolin B functions

as a Hippo regulator through the activation of LATS (large tumor suppressor) kinases (drug-induced phosphorylation of LATS at T1079) and the downstream phosphorylation of YAP/TAZ transcriptional coactivators to suppress gene expression and cell growth. The initial Michael reaction of microcolin B with the thiol group of Cys94 in PITPβ is essential. The dihydro analog of microcolin B is an inactive compound [19]. The activation of the tumor-suppressive Hippo–YAP/TAZ signaling pathway to promote Yap degradation is viewed as a promising approach to the inhibition of tumorigenesis [24]. There are multiple strategies to target the Hippo pathway with small molecules [25,26], but the use of microcolins and derivatives is a unique option for targeting PITPα/β. A recent study using chemical proteomic methods revealed that the derivative microcolin H, also produced by *Moorea producens*, directly binds the two isoforms PITPα and PITPβ similarly so as to induce autophagic cell death and reduce tumor growth in mice [27].

These considerations prompted us to investigate the binding of microcolins to PITP using molecular modeling to help identify the best binders in the series and facilitate the design of analogs. We compared the PITP interaction of microcolins A-M and VT01454 using the high-resolution (2.2 Å) structure of a phosphatidylcholine-bound PITPα isoform found via X-ray diffraction (Protein Data Bank (PDB) entry 1T27) [28]. This structure has been used by others to investigate the PITPα phosphatidylinositol–phosphatidylcholine lipid exchange cycle [29] and to study the binding of ursolic acid to PITPα [30]. It is a representative PITP. A structure comparison of the α and β PITP isoforms revealed minimal differences in protein conformation [31]. Here, we used the same structure to study the binding of microcolins to the PITPα phosphatidylcholine binding site.

2. Materials and Methods

2.1. Protein Structures, Programs and Process

Different tridimensional structures of phosphatidylinositol transfer proteins (PITPs) are available in the Protein Data Bank (PDB, www.rcsb.org accessed on 11 January 2025). The structure of PITPα in complex with phosphatidylcholine (1T27) was selected for its good resolution and because it has been used in previous binding studies [28]. A molecular docking analysis was performed with Genetic Optimization for Ligand Docking (GOLD) 5.3 software (Cambridge Crystallographic Data Centre, Cambridge, UK). A Monte Carlo conformational searching procedure was conducted using BOSS v4.9 software to optimize the structure of each ligand prior to the docking analysis [32]. The 2D-3D structures of the natural products were retrieved from the PubChem database or built from the original publications describing the compounds (Figure 1). Molecular graphic analyses were performed using Discovery Studio Visualizer, Biovia 2020 (Dassault Systèmes BIOVIA Discovery Studio Visualizer 2020, San Diego, CA, USA, Dassault Systèmes, 2020).

2.2. Protein–Ligand Binding Site Prediction

Potential–ligand binding sites on the PITPα protein were identified using the web server Computed Atlas of Surface Topography of proteins (CASTp) 3.0 [33]. This software is used to predict the position of ligand binding sites with an estimated success rate of 74% [34]. This method analyzes the protein geometry to identify and measure pockets and voids on 3D protein structures, with the support of the modeling software Chimera 1.15 for visualization [35]. It is an efficient method for modeling protein secondary structures and analyzing the distribution of essential amino acid residues involved in binding interactions [36,37].

2.3. Molecular Docking Analysis

The phosphatidylcholine binding area within the PITPα protein structure was considered as the potential binding site for the studied products. To incorporate protein flexibility into the docking process, the side chains of 10 key amino acids implicated in the binding process were rendered fully flexible. For protein PITPα (1T27), these amino acids were Tyr63, His64, Cys95, Phe108, Phe201, Trp203, Phe213, Phe222, Phe225 and His226. For protein PITPβ (2A1L) [31], the flexible amino acids were Val26, Tyr62, Leu64, Phe83, Phe107, Phe212, Ile220, Phe221, Leu224 and His225. With each protein, a central amino acid was defined based on shape complementarity and geometry to delimit a docking grid. With both proteins and each alkaloid, the binding mode was analyzed considering 100 energetically reasonable poses which were then selected and ranked. The fitness scoring function was used to rank the 6 best binding poses, based on the Piecewise Linear Potential (PLP) fitness value, a pairwise additive scoring function incorporated into GOLD [38]. Then, from the best PLP fitness scores, the binding energies were calculated. No rescoring of binding affinities was performed.

For each ligand, the empirical potential energy of the interaction (ΔE) was calculated using the SPASIBA spectroscopic force field, via the expression ΔE(interaction) = E(complex) − [E(protein) + E(ligand)]. The Boss program and the Molecular Mechanics/Generalized Born Surface Area (MM/GBSA) procedure were used to calculate the free energies of hydration (ΔG) in relation to aqueous solubility [39]. MM/GBSA does not provide information about the number, position or free energy of water molecules, but the contribution of water molecules in the binding site is estimated in the calculation of Gibb's free energy of binding (ΔG) values [40]. The SPASIBA force field (integrated into CHARMM v36) correctly reproduces crystal phase infrared data. It was developed to provide refined empirical molecular mechanics force field parameters, as described in other studies [41,42]. This specific force field for Monte Carlo (MC) simulations achieved the same level of convergence as Molecular Dynamics (MD), with less computation time [43].

3. Results

3.1. PITPα Protein: Topographic Analysis of Drug Binding Site

The PITPα protein presents a large central cavity for drug binding. Its natural ligand phosphatidylcholine binds well into this site, occupying the free space between the β-sheet portion and the proximal α-helices (Figure 2a). The drug binding site is thus delimited. Nevertheless, the surface topography of the protein was analyzed using the CASTp server, which is a convenient online service for identifying, defining and quantifying the geometric and topological features of protein structures, notably the surface pocket and the volume of interior cavities [33,34]. The analysis with CASTp revealed a single suitable cavity for drug binding. It corresponds to a large site with a volume and area of the pocket of 621 $Å^3$ and 923 $Å^2$, respectively, suitable for comfortably accommodating extended small molecules like microcolins. The other potential binding pockets were far too small (Figure 2b). Therefore, the main zone (shown in red) generated by the CASTp server was defined as the microcolin binding zone, delimited by the ten flexible amino acid residues Tyr63, His64, Cys95, Phe108, Phe201, Trp203, Phe213, Phe222, Phe225 and His226.

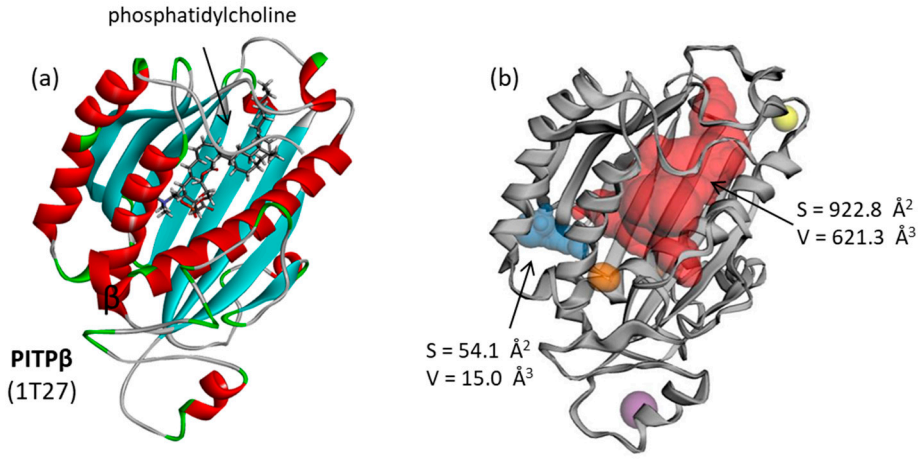

Figure 2. A binding site analysis of PITPα using the web server CASTp 3.0. (**a**) The analysis of the full-length protein (1T27) shows the phosphatidylcholine binding site located over the β-sheet portion of the protein (in blue). (**b**) A CAST analysis of PITPα, with the identification of the large binding cavity (in red), with the indicated surface (S) and volume (V). Minor areas are identified around the protein (small areas colored in blue, purple, orange and yellow).

3.2. Binding of Microcolins to PITPα: Docking Study

A molecular docking analysis was performed from structure 1T27 after the removal of the phosphatidylcholine molecule to allow the test molecule to have free access to the central cavity centered around position Phe108. The analysis was repeated with each microcolin compound to calculate the empirical energy of interaction (ΔE) and free energy of hydration (ΔG). Data obtained with VT01454 and microcolins are collated in Table 1. The large cavity in the protein allowed for the facile binding of natural products. Out of the 13 microcolins, 5 compounds gave ΔE < −100 kcal/mol: microcolins A, B, E, G, H and L. Overall, the two best compounds in the series were microcolin E and VT01454. ΔE values provide an indication of the complex stability and ΔG values an estimate of the ligand binding affinity. The MM/GBSA binding free energy score (solvation-dependent Gibb's free energy of binding, ΔG) was considered to select the best molecules.

Table 1. Calculated potential energy of interaction (ΔE) and free energy of hydration (ΔG) for interaction of microcolins with PITPα.

Compounds	ΔE (kcal/mol)	ΔG (kcal/mol)
Phosphatidylcholine	−163.80	−44.95
Microcolin A	−103.10	−40.35
Microcolin B	−107.35	−34.55
Microcolin C	−96.40	−43.20
Microcolin D	−98.50	−40.00
Microcolin E	−116.60	−39.70
Microcolin F	−98.20	−37.70
Microcolin G	−100.60	−36.85
Microcolin H	−107.20	−32.80
Microcolin I	−98.15	−35.20
Microcolin J	−97.60	−39.75
Microcolin K	−94.60	−36.80
Microcolin L	−100.70	−32.30
Microcolin M	−99.40	−33.80
Majusculamide D	−109.65	−39.30
Deoxy-majuscul. D	−107.70	−41.20
VT01454	−111.70	−43.50

Figure 3 shows the binding of microcolins B and H to PITPα. They display a comparable protein binding mode with the lactam extremity deeply inserted into the protein cavity and the dimethyloctanoyl moiety lying on the β-sheets on the other side of the binding site. In both cases, the drug molecule is well protected in the protein cavity, but its central part remains fairly accessible to the solvent (Figure 3b,d). The tripeptide portion of the molecule sits on the β-sheet bed and positions the pyrrolidine unit near the reactive site. Both microcolins B and H establish numerous contacts with the protein, as illustrated in Figure 4.

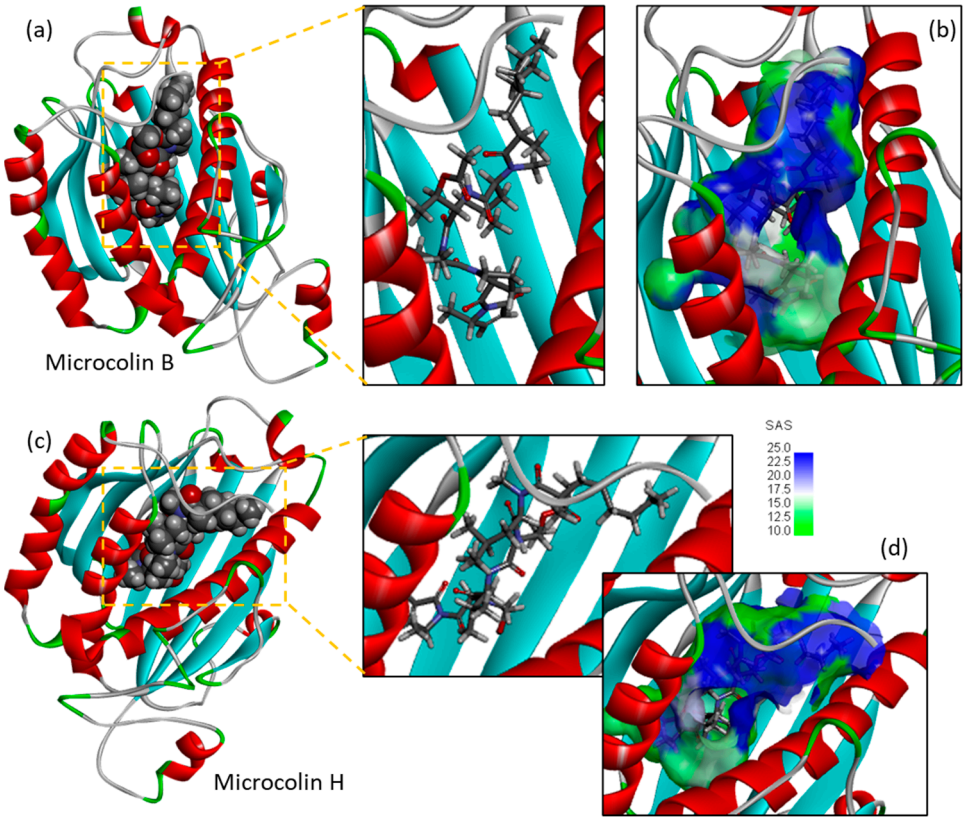

Figure 3. The binding of microcolins B and H to PITPα. (**a**) A ribbon model of microcolin B bound to PITPα with a detailed view of the interaction site. The β-sheets (in blue) and α-helices (in red) are shown. (**b**) The solvent-accessible surface (SAS) surrounding the drug binding zone (color code indicated). (**c**,**d**) The same models for microcolin H.

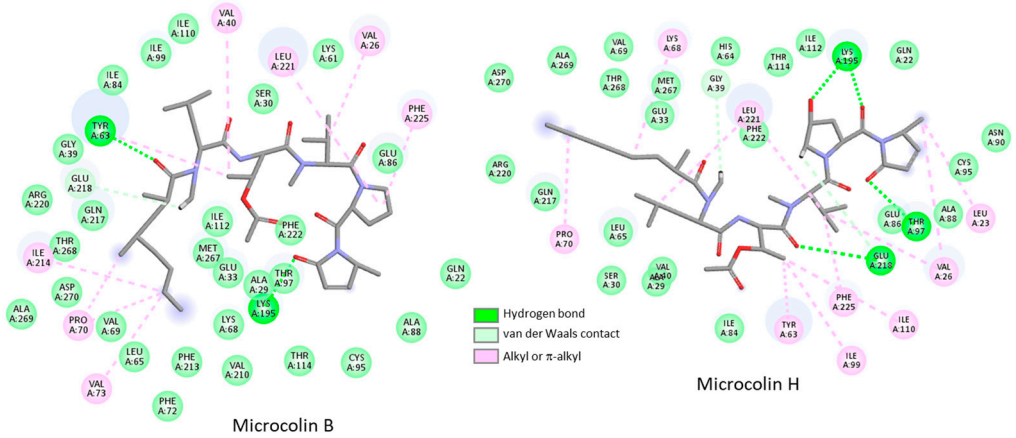

Figure 4. Binding map contacts for microcolins B and H bound to PITPα (color code indicated).

There are over 35 contacts between microcolin B and PITPα, including two key H-bonds with residues Tyr63 and Lys195. These are the two most important contacts, observed with almost all microcolin derivatives. The binding situation is a little similar to that for microcolin H, which exploits residues Glu218 and Lys195 for binding, in a manner close to that observed with compound VT01454 (Figure 5). The mode of binding of microcolins B and E to PITPα is relatively similar, with about 38 protein contacts in both cases (Figure 6). The two products make use of the large protein bed to occupy all of the groove and robustly anchor their tripeptide portion into the cavity. In each case, multiple van der Waals contacts stabilize the protein–drug complex.

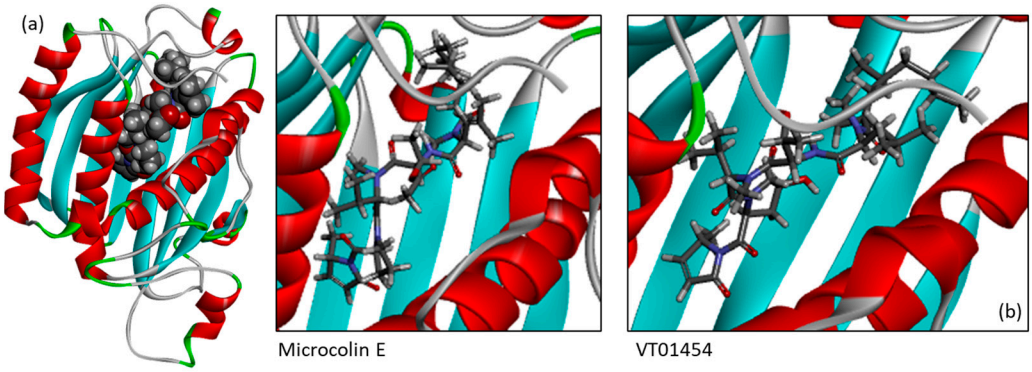

Figure 5. Molecular models of (**a**) microcolin E and (**b**) VT01454 bound to PITPα. Other details are same as those for Figure 3.

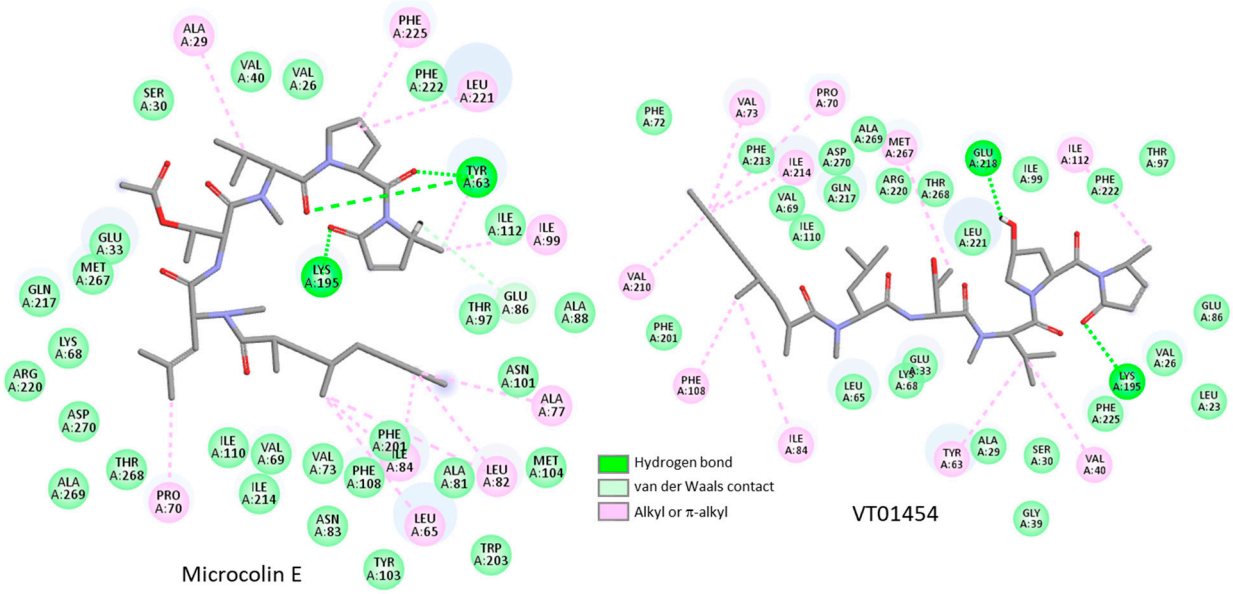

Figure 6. Binding map contacts for microcolin E and VT01454 bound to PITPα (color code indicated).

A comparison of the binding energies calculated with the different microcolins permits us to deduce at least four pieces of structural information. First, the acetyl group at position R_2 on microcolins A and B positively contributes to the protein interaction. The deacetylated derivatives microcolin C (desacetyl-microcolin B) and microcolin D (desacetyl-microcolin A) are weaker binders than the acetylated analogs. Second, the hydroxyl group on the pyrrolidine unit is not an essential element for protein binding. Microcolin B (R_1 = H) is a better binder than microcolin A (R_1 = OH), and the same observation is made when comparing microcolin E (R_1 = H) and microcolin F (R_1 = OH). The calculated binding energy is largely in favor of microcolin E versus microcolin F. However, the opposite

was observed when comparing microcolin I (R_1 = H) and microcolin H (R_1 = OH). Third, the truncated derivative, microcolin M, which lacks the terminal lactam unit, binds less efficiently to the protein. This suggests that the lactam unit is important for binding or for bonding, as discussed below. The pentanoyl side chain common to microcolins A-B can be replaced with a pentenoyl chain as in microcolins E–F or with a hexanoyl chain as in microcolin L. Apparently, the change at this position has little impact on PITPα binding. Fourth, the comparison of microcolins B and J suggests that the N-methyl substituent contributes favorably to the protein interaction. A surprising observation derives from the comparison of the two compound isomers microcolin D and VT01454, which only differ by the orientation of their 2,4-dimethyloctanamide side chain, as shown in Figure 7. VT01454 appears to be a much better PITPα binder than microcolin D (Table 1). This structure–binding information is important for searching for additional compounds susceptible to binding to PITP and for drug design.

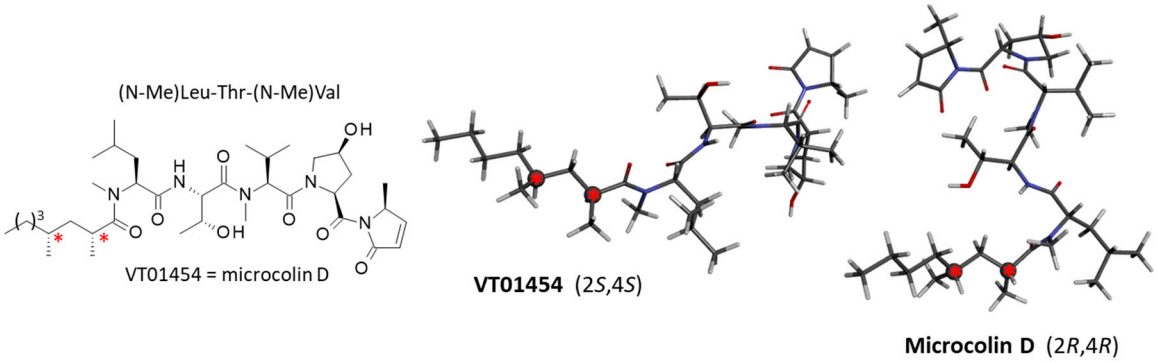

Figure 7. Structural comparison of two isomers VT01454 and microcolin D.

3.3. Covalent Binding of Microcolin H to PITP

A comparison of the binding configuration observed with the different microcolins revealed the proximity of the reactive electrophilic α,β-unsaturated ketone to the thiol nucleophilic group of the amino acid Cys95 of PITPα. This is best illustrated in the case of microcolin H, with a distance of 3.2 Å between the nucleophilic free thiol Cys95-SH and the β-carbon of the α,β-unsaturated ketone. The reactive group is ideally located for covalent binding to the cysteine residue. The nucleophilic addition reaction of sulfhydryl toward the α,β-unsaturated ketone was simulated to obtain the covalent adduct, as shown in Figure 8. After reaction, the measured C-S distance was reduced to 1.8 Å, with a slight movement of the reactive unit. The rest of the molecule remained stabilized in the protein cavity. A similar sulfhydryl adduction of Cys95 can occur with the other derivatives, notably with microcolin B for which the methyl-dihydropyrrolone unit is engaged in a van der Waals contact with Cys95 (Figure 4).

The facile covalent binding of microcolin H to Cys95 of PITPα is entirely consistent with the experimental data reported by Yang and coworkers using a chemical proteomic approach [27]. Rat PITPβ models (pdb: 2A1L) showed a covalent attachment of microcolin H to Cys94, equivalent to Cys95 in the structure of rat PITPα (pdb: 1T27) used here. Our own study of the binding of microcolin H to PITPβ showed no major difference with PITPα. The modeling analysis showed the good stability of microcolin H-PITPβ complexes (Figure S1). The energy parameters were even more favorable with PITPβ compared to PITPα (1T27) (ΔE = −119.95 kcal/mol and ΔG = −41.60 kcal/mol for PITPβ (2A1L) vs. ΔE = −107.20 kcal/mol and ΔG = −32.80 kcal/mol PITPα (1T27). The structures of the two isoforms are superimposable [31]. Microcolin H can easily form covalent complexes with PITPβ through binding to the thiol group of Cys94 (Figure S2). It is also interesting to note

that our model is fully consistent with a crystallographic structure of inhibitor VT01454 covalently attached to the Cys95 of PITPα (pdb: 8PQO) [44] (Figure S3).

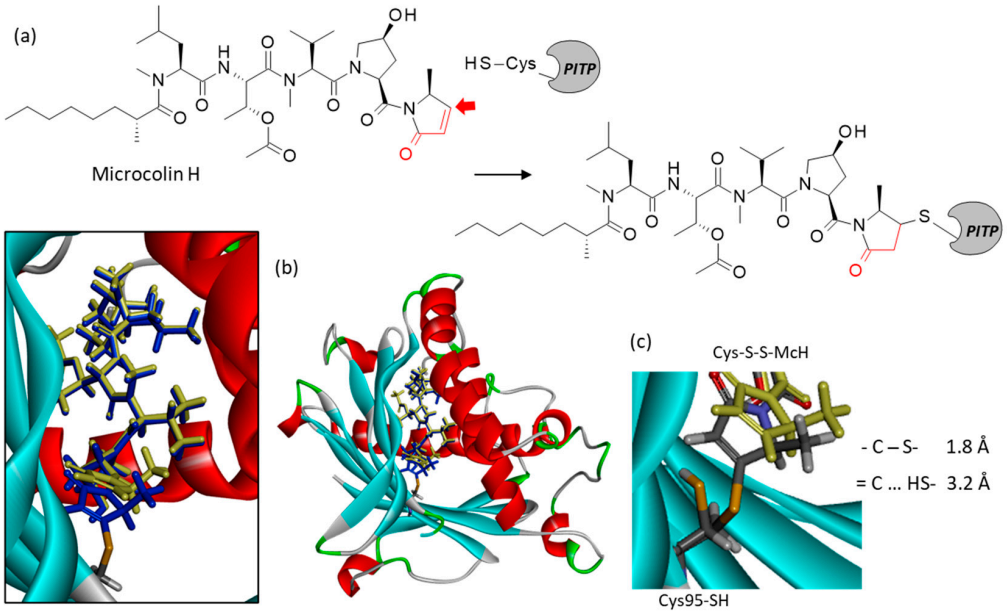

Figure 8. The covalent binding of microcolin H to PITPα. (**a**) The reaction process, with the reactive site (in red). (**b**) Models of the product bound to the protein in a non-covalent (in yellow) and covalent (in blue) form. (**c**) A detailed view of the portion of PITPα bound to the SH group of residue Cys95. The covalent and non-covalent forms are shown, with the C–S measured distances.

3.4. Binding of Related Natural Products to PITPβ

Based on the above structural information, we searched for related natural products which could also interact with the protein. We identified two compounds: majusculamide D and its deoxy analog (Figure 9). Majusculamide D and deoxy-majusculamide D are two lipopentapeptides originally isolated from *Lyngbya majuscula* and later found in *Moorea* species [45]. They are structurally close to microcolins, with a N,O-dimethyltyrosine in place of a N-methylleucine residue in the central tripeptide motif.

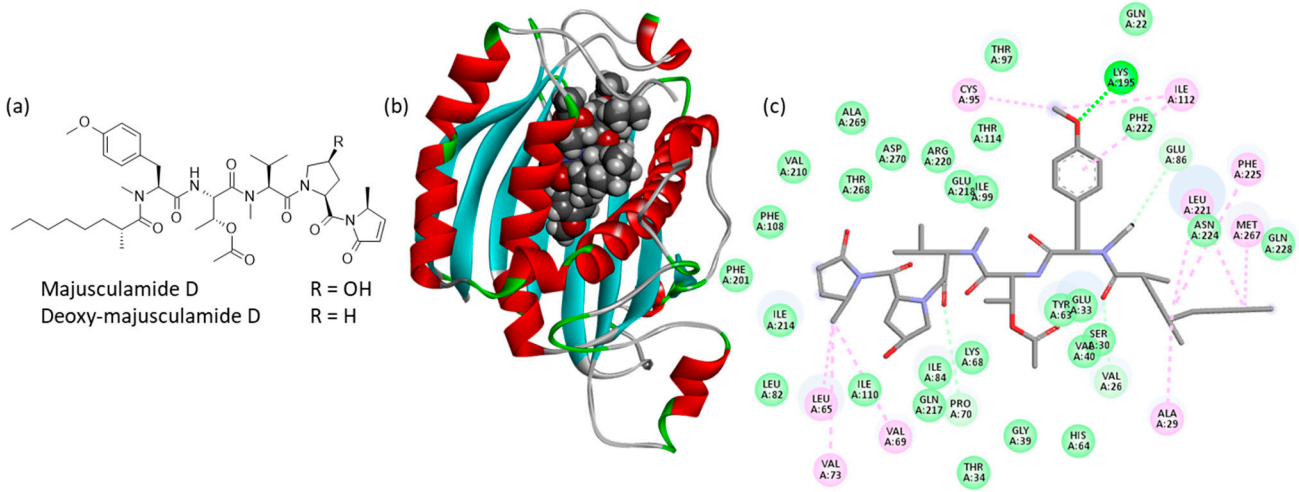

Figure 9. (**a**) Structure of majusculamide D and its deoxy analog. (**b**) Binding of majusculamide D to PITPα with (**c**) molecular contacts between drug and protein (color code as in Figure 6).

The total synthesis of majusculamide D was accomplished, and the product revealed prominent cytotoxic activity against PANC1 pancreatic cancer cells in vitro (IC_{50} = 0.32 nM) [46].

A recent study using synthetic majusculamide D derivatives demonstrated that both the hydroxyl group at C10 and C2–C3 unsaturated double bond were essential in maintaining high activity levels against PANC1 cells [47,48]. Here, we observed that both majusculamide D and deoxy-majusculamide D can form stable complexes with PITPα, with little difference between the two compounds. Majusculamide D formed the most stable protein complexes, largely engaging its tyrosine residue in the interaction. A H-bond between Lys195 and the methoxyphenyl group of the drug contributes to the stability of the protein–drug complex.

4. Discussion

The marine filamentous cyanobacterium *Moorena producens*, also named *Lyngbya majuscula*, produces numerous secondary metabolites utilized for its own metabolism and/or for its defense against predators. It produces poisoning metabolites to many marine organisms, notably shrimps and turtles [4]. This cyanobacterium is known to cause skin irritation, possibly leading to seaweed dermatitis [2]. But some of these secondary metabolites present a pharmacological interest in terms of the treatment of cancers and other severe diseases. For example, a recent study explored the antiparasitic activity of metabolites from *M. producens* and identified different peptides (almiramides, dragonamides) active against *Leishmania donovani*, *Trypanosoma cruzi* and *T. brucei* parasites [49,50]. The products isolated are not necessarily toxic. For example, a recent work identified the lipopeptide kalkitoxin and showed its capacity to decrease vascular calcification, making it of potential interest for treating arteriosclerosis [51,52]. The same product may be useful in treating cancer and metastasis based on its capacity to protect from osteolysis [9]. Therefore, it is essential to characterize the mechanism of action of such lipopeptides well to make use of their pharmacological properties. Once the mechanism of action is explored or defined, the compounds in the series can be exploited to design drug candidates. For example, the discovery of cytotoxic lagunamides from *M. producens* [53] was followed by the characterization of their anticancer mechanism of action and the synthesis of analogs [54–56]. Numerous lipopeptides isolated from *M. producens* have been characterized, but for many of them, their mechanism of action remains little known at present.

The microcolin series of products isolated from *M. producens* is interesting, structurally and functionally, notably because their anticancer effects have been investigated well. The molecular targets of the lead products in the series, microcolins B and H, have been clearly identified as being the phosphatidylinositol transfer proteins PITPα/β. Microcolin B and its analog VT01454 were shown to target PITPα/β, thereby inducing the phosphorylation of the YAP protein and inactivation through the Hippo pathway [19]. Similarly, microcolin H was shown to bind directly to PITPα/β [27]. These proteins involved in the regulation of phosphoinositide synthesis play a role in cancer cell survival and proliferation. They are also implicated in diverse PITP-driven pathologies such as neurodegeneration, immunity and metabolic diseases [19,57]. For these reasons, small-molecule PITP inhibitors are being actively investigated [58]. A better understanding of the structure–binding relationships in the microcolin series can help in the design of novel inhibitors. Diverse approaches have been described to synthesize these lipopeptides, notably for microcolins A and B [59–63]. Molecular modeling can help to guide the design of analogs and prioritize the compounds. The docking analysis reported here confirms the interest in microcolins B and H as robust ligands of PITPα/β and reveals the potential of microcolin E as being the best ligand of PITPα in the series. It also underlines the possibility of using VT01454 and majusculamide D as templates to design PITP inhibitors. The structure–binding relationships reported here shall be an aid to the discovery of novel PITP binders.

PITPα/β are perhaps not the unique targets of microcolins, but these two proteins represent the primary components of their mechanism of action. Thus far, there is little

evidence that microcolins can affect PITP-independent pathways. An in silico study raised the idea that cytotoxic products from *Lyngbya majuscula*, including majusculamide D (but not microcolins), could interfere with cancer cell growth through binding to heat-shock protein 90 (Hsp90 chaperone) [64]. But at present, PITPα/β remain the only validated targets for microcolins.

5. Conclusions

This molecular docking study identified PITPα/β as protein targets for the marine lipopeptides microcolins. Structure–binding relationships were identified. The best ligands in the series are microcolins E, B and H, susceptible to forming covalent complexes with a cysteine residue via their common electrophilic α,β-unsaturated ketone group. Among the many natural products of pharmacological interest produced by marine cyanobacteria, microcolins represent good lead compounds for the design of anticancer agents [65]. Hopefully, the computational study reported here will encourage pharmacologists to further investigate the binding of microcolins to PITB and the biological consequences of this interaction for the treatment of cancers and other pathologies for which PITPα/β play a significant role.

Supplementary Materials: The following supporting information can be downloaded at https://www.mdpi.com/article/10.3390/futurepharmacol5010013/s1, Figure S1: Binding of microcolin H to PITPβ; Figure S2: Superimposed models of microcolin H bound to PITPβ in non-covalent and covalent forms; Figure S3: Crystallographic structure of inhibitor VT01454 covalently linked to Cys95 of PITPα.

Author Contributions: Conceptualization, C.B.; methodology, G.V.; software, G.V.; investigation, C.B.; data curation, C.B.; writing—original draft preparation, C.B.; writing—review and editing, C.B.; visualization, C.B. and G.V. All authors have read and agreed to the published version of the manuscript.

Funding: This research received no external funding.

Institutional Review Board Statement: Not applicable.

Informed Consent Statement: Not applicable.

Data Availability Statement: Data are contained within the article and Supplementary Materials.

Conflicts of Interest: The authors declare no conflicts of interest. OncoWitan is the scientific consulting office of Christian Bailly. This company had no role in the design of the study; in the collection, analyses or interpretation of data; in the writing of the manuscript; or in the decision to publish the results.

Abbreviations

The following abbreviations are used in this manuscript:

LATS	Large tumor suppressor
PITP	Phosphatidylinositol transfer protein
TAZ	Transcriptional coactivator with PDZ-binding motif
YAP	Yes-associated protein

References

1. Sharp, K.; Arthur, K.E.; Gu, L.; Ross, C.; Harrison, G.; Gunasekera, S.P.; Meickle, T.; Matthew, S.; Luesch, H.; Thacker, R.W.; et al. Phylogenetic and chemical diversity of three chemotypes of bloom-forming lyngbya species (Cyanobacteria: Oscillatoriales) from reefs of southeastern Florida. *Appl. Environ. Microbiol.* **2009**, *75*, 2879–2888. [CrossRef] [PubMed]
2. Hill, K.L.; Fulton, H.M.; McGovern, T.W. Aquatic Antagonists: Seaweed Dermatitis (*Lyngbya majuscula*). *Cutis* **2024**, *113*, E38–E40. [CrossRef] [PubMed]

3. Curren, E.; Leong, S.C.Y. Global phylogeography of toxic cyanobacteria *Moorea producens* reveals distinct genetic partitioning influenced by Proterozoic glacial cycles. *Harmful Algae* **2019**, *86*, 10–19. [CrossRef]
4. Curren, E.; Leaw, C.P.; Lim, P.T.; Leong, S.C.Y. The toxic cosmopolitan cyanobacteria *Moorena producens*: Insights into distribution, ecophysiology and toxicity. *Environ. Sci. Pollut. Res. Int.* **2022**, *29*, 78178–78206. [CrossRef]
5. Ngo, T.E.; Ecker, A.; Ryu, B.; Guild, A.; Remmel, A.; Boudreau, P.D.; Alexander, K.L.; Naman, C.B.; Glukhov, E.; Avalon, N.E.; et al. Structure and Biosynthesis of Hectoramide B, a Linear Depsipeptide from Marine Cyanobacterium *Moorena producens* JHB Discovered via Coculture with *Candida albicans*. *ACS Chem. Biol.* **2024**, *19*, 619–628, Correction in *ACS Chem. Biol.* **2024**, *19*, 2593. [CrossRef]
6. Youssef, D.T.A.; Mufti, S.J.; Badiab, A.A.; Shaala, L.A. Anti-Infective Secondary Metabolites of the Marine Cyanobacterium Lyngbya Morphotype between 1979 and 2022. *Mar. Drugs* **2022**, *20*, 768. [CrossRef]
7. Levert, A.; Alvariño, R.; Bornancin, L.; Abou Mansour, E.; Burja, A.M.; Genevière, A.M.; Bonnard, I.; Alonso, E.; Botana, L.; Banaigs, B. Structures and Activities of Tiahuramides A-C, Cyclic Depsipeptides from a Tahitian Collection of the Marine Cyanobacterium *Lyngbya majuscula*. *J. Nat. Prod.* **2018**, *81*, 1301–1310. [CrossRef]
8. Sweeney-Jones, A.M.; Gagaring, K.; Antonova-Koch, J.; Zhou, H.; Mojib, N.; Soapi, K.; Skolnick, J.; McNamara, C.W.; Kubanek, J. Antimalarial Peptide and Polyketide Natural Products from the Fijian Marine Cyanobacterium *Moorea producens*. *Mar. Drugs* **2020**, *18*, 167. [CrossRef]
9. Shrestha, S.K.; Min, K.H.; Kim, S.W.; Kim, H.; Gerwick, W.H.; Soh, Y. Kalkitoxin: A Potent Suppressor of Distant Breast Cancer Metastasis. *Int. J. Mol. Sci.* **2023**, *24*, 1207. [CrossRef]
10. Kawaguchi, M.; Satake, M.; Zhang, B.T.; Xiao, Y.Y.; Fukuoka, M.; Uchida, H.; Nagai, H. Neo-Aplysiatoxin A Isolated from Okinawan Cyanobacterium *Moorea producens*. *Molecules* **2020**, *25*, 457. [CrossRef]
11. Semmouri, I.; Janssen, C.R.; Asselman, J. Health risks associated with the consumption of sea turtles: A review of chelonitoxism incidents and the presumed responsible phycotoxins. *Sci. Total Environ.* **2024**, *954*, 176330. [CrossRef]
12. Pearson, L.A.; Karuso, P.; Neilan, B.A. Structure, biosynthesis and activity of indolactam alkaloids. *Alkaloids Chem. Biol.* **2024**, *92*, 1–45. [PubMed]
13. Yu, H.B.; Glukhov, E.; Li, Y.; Iwasaki, A.; Gerwick, L.; Dorrestein, P.C.; Jiao, B.H.; Gerwick, W.H. Cytotoxic Microcolin Lipopeptides from the Marine Cyanobacterium *Moorea producens*. *J. Nat. Prod.* **2019**, *82*, 2608–2619. [CrossRef] [PubMed]
14. Koehn, F.E.; Longley, R.E.; Reed, J.K. Microcolins A and B, new immunosuppressive peptides from the blue-green alga *Lyngbya majuscula*. *J. Nat. Prod.* **1992**, *55*, 613–619. [CrossRef] [PubMed]
15. Zhang, L.H.; Longley, R.E.; Koehn, F.E. Antiproliferative and immunosuppressive properties of microcolin A, a marine-derived lipopeptide. *Life Sci.* **1997**, *60*, 751–762. [CrossRef]
16. Zhang, L.H.; Longley, R.E. Induction of apoptosis in mouse thymocytes by microcolin A and its synthetic analog. *Life Sci.* **1999**, *64*, 1013–1028. [CrossRef]
17. Koehn, F.E.; McConnell, O.J.; Longley, R.E.; Sennett, S.H.; Reed, J.K. Analogues of the marine immunosuppressant microcolin A: Preparation and biological activity. *J. Med. Chem.* **1994**, *37*, 3181–3186. [CrossRef]
18. Mandal, A.K.; Hines, J.; Kuramochi, K.; Crews, C.M. Developing microcolin A analogs as biological probes. *Bioorg. Med. Chem. Lett.* **2005**, *15*, 4043–4047. [CrossRef]
19. Li, F.L.; Fu, V.; Liu, G.; Tang, T.; Konradi, A.W.; Peng, X.; Kemper, E.; Cravatt, B.F.; Franklin, J.M.; Wu, Z.; et al. Hippo pathway regulation by phosphatidylinositol transfer protein and phosphoinositides. *Nat. Chem. Biol.* **2022**, *18*, 1076–1086. [CrossRef]
20. Hamaï, A.; Drin, G. Specificity of lipid transfer proteins: An in vitro story. *Biochimie* **2024**, *227*, 85–110. [CrossRef]
21. Allen-Baume, V.; Ségui, B.; Cockcroft, S. Current thoughts on the phosphatidylinositol transfer protein family. *FEBS Lett.* **2002**, *531*, 74–80. [CrossRef] [PubMed]
22. Pathak, A.; Willis, K.G.; Bankaitis, V.A.; McDermott, M.I. Mammalian START-like phosphatidylinositol transfer proteins—Physiological perspectives and roles in cancer biology. *Biochim. Biophys. Acta Mol. Cell Biol. Lipids* **2024**, *1869*, 159529. [CrossRef] [PubMed]
23. Zhu, R.; Jiao, Z.; Yu, F.X. Advances towards potential cancer therapeutics targeting Hippo signaling. *Biochem. Soc. Trans.* **2024**, *52*, 2399–2413. [CrossRef]
24. Hu, D.; Meng, R.Y.; Nguyen, T.V.; Chai, O.H.; Park, B.H.; Lee, J.S.; Kim, S.M. Inhibition of colorectal cancer tumorigenesis by ursolic acid and doxorubicin is mediated by targeting the Akt signaling pathway and activating the Hippo signaling pathway. *Mol. Med. Rep.* **2023**, *27*, 11. [CrossRef]
25. Li, N.; Liu, Y.H.; Wu, J.; Liu, Q.G.; Niu, J.B.; Zhang, Y.; Fu, X.J.; Song, J.; Zhang, S.Y. Strategies that regulate Hippo signaling pathway for novel anticancer therapeutics. *Eur. J. Med. Chem.* **2024**, *276*, 116694. [CrossRef]
26. Koroleva, O.A.; Kurkin, A.V.; Shtil, A.A. The Hippo pathway as an antitumor target: Time to focus on. *Expert. Opin. Investig. Drugs* **2024**, *33*, 1177–1185. [CrossRef]
27. Yang, H.; Zhang, X.; Wang, C.; Zhang, H.; Yi, J.; Wang, K.; Hou, Y.; Ji, P.; Jin, X.; Li, C.; et al. Microcolin H, a novel autophagy inducer, exerts potent antitumour activity by targeting PITPalpha/beta. *Signal Transduct. Target. Ther.* **2023**, *8*, 428. [CrossRef]

28. Yoder, M.D.; Thomas, L.M.; Tremblay, J.M.; Oliver, R.L.; Yarbrough, L.R.; Helmkamp, G.M., Jr. Structure of a multifunctional protein. Mammalian phosphatidylinositol transfer protein complexed with phosphatidylcholine. *J. Biol. Chem.* **2001**, *276*, 9246–9252. [CrossRef]
29. Grabon, A.; Orłowski, A.; Tripathi, A.; Vuorio, J.; Javanainen, M.; Róg, T.; Lönnfors, M.; McDermott, M.I.; Siebert, G.; Somerharju, P.; et al. Dynamics and energetics of the mammalian phosphatidylinositol transfer protein phospholipid exchange cycle. *J. Biol. Chem.* **2017**, *292*, 14438–14455. [CrossRef]
30. Biswas, S.; Mukherjee, P.K.; Harwansh, R.K.; Bannerjee, S.; Bhattacharjee, P. Enhanced bioavailability and hepatoprotectivity of optimized ursolic acid-phospholipid complex. *Drug Dev. Ind. Pharm.* **2019**, *45*, 946–958. [CrossRef]
31. Vordtriede, P.B.; Doan, C.N.; Tremblay, J.M.; Helmkamp, G.M., Jr.; Yoder, M.D. Structure of PITPbeta in complex with phosphatidylcholine: Comparison of structure and lipid transfer to other PITP isoforms. *Biochemistry* **2005**, *44*, 14760–14771. [CrossRef] [PubMed]
32. Jorgensen, W.L.; Tirado-Rives, J. Molecular modeling of organic and biomolecular systems using BOSS and MCPRO. *J. Comput. Chem.* **2005**, *26*, 1689–1700. [CrossRef] [PubMed]
33. Tian, W.; Chen, C.; Lei, X.; Zhao, J.; Liang, J. CASTp 3.0: Computed atlas of surface topography of proteins. *Nucleic Acids Res.* **2018**, *46*, 363–367. [CrossRef] [PubMed]
34. Huang, B.; Schroeder, M. LIGSITEcsc: Predicting ligand binding sites using the Connolly surface and degree of conservation. *BMC Struct. Biol.* **2006**, *6*, 19. [CrossRef]
35. Dundas, J.; Ouyang, Z.; Tseng, J.; Binkowski, A.; Turpaz, Y.; Liang, J. CASTp: Computed atlas of surface topography of proteins with structural and topographical mapping of functionally annotated residues. *Nucleic Acids Res.* **2006**, *34*, W116–W118. [CrossRef]
36. Zhao, J.; Cao, Y.; Zhang, L. Exploring the computational methods for protein-ligand binding site prediction. *Comput. Struct. Biotechnol. J.* **2020**, *18*, 417–426. [CrossRef]
37. Prymula, K.; Jadczyk, T.; Roterman, I. Catalytic residues in hydrolases: Analysis of methods designed for ligand-binding site prediction. *J. Comput. Aided Mol. Des.* **2011**, *25*, 117–133. [CrossRef]
38. Jones, G.; Willett, P.; Glen, R.C.; Leach, A.R.; Taylor, R. Development and validation of a genetic algorithm for flexible docking. *J. Mol. Biol.* **1997**, *267*, 727–748. [CrossRef]
39. Meziane-Tani, M.; Lagant, P.; Semmoud, A.; Vergoten, G. The SPASIBA force field for chondroitin sulfate: Vibrational analysis of D-glucuronic and N-acetyl-D-galactosamine 4-sulfate sodium salts. *J. Phys. Chem. A* **2006**, *110*, 11359–11370. [CrossRef]
40. Genheden, S.; Ryde, U. The MM/PBSA and MM/GBSA methods to estimate ligand-binding affinities. *Expert. Opin. Drug Discov.* **2015**, *10*, 449–461. [CrossRef]
41. Lagant, P.; Nolde, D.; Stote, R.; Vergoten, G.; Karplus, M. Increasing normal modes analysis accuracy: The SPASIBA spectroscopic force field introduced into the CHARMM program. *J. Phys. Chem. A* **2004**, *108*, 4019–4029. [CrossRef]
42. Vergoten, G.; Mazur, I.; Lagant, P.; Michalski, J.C.; Zanetta, J.P. The SPASIBA force field as an essential tool for studying the structure and dynamics of saccharides. *Biochimie* **2003**, *85*, 65–73. [CrossRef] [PubMed]
43. Jorgensen, W.L.; Tirado-Rives, J. Monte Carlo versus Molecular Dynamics for conformational sampling. *J. Phys. Chem.* **1996**, *100*, 14508–14513. [CrossRef]
44. Kim, Y.J.; Pemberton, J.G.; Eisenreichova, A.; Mandal, A.; Koukalova, A.; Rohilla, P.; Sohn, M.; Konradi, A.W.; Tang, T.T.; Boura, E.; et al. Non-vesicular phosphatidylinositol transfer plays critical roles in defining organelle lipid composition. *EMBO J.* **2024**, *43*, 2035–2061. [CrossRef]
45. Moore, R.E.; Entzeroth, M. Majusculamide D and deoxymajusculamide D, two cytotoxins from *Lyngbya majuscula*. *Phytochemistry* **1988**, *27*, 3101–3103. [CrossRef]
46. Caro-Diaz, E.J.E.; Valeriote, F.A.; Gerwick, W.H. Highly Convergent Total Synthesis and Assignment of Absolute Configuration of Majusculamide D, a Potent and Selective Cytotoxic Metabolite from *Moorea* sp. *Org. Lett.* **2019**, *21*, 793–796, Correction in Org. Lett. **2020**, *22*, 6220. [CrossRef]
47. Zhao, X.; Xi, X.; Zhang, M.; Lv, M.; Zhang, X.; Lu, Y.; Wang, L.; Chen, Y. Structure-Activity Relationship Study of Majusculamide D: Overcoming Metabolic Instability and Severe Toxicity with a Fluoro Analogue. *Mar. Drugs* **2024**, *22*, 537. [CrossRef]
48. Zhao, X.; Lv, M.; Xi, X.; Lu, Y.; Wang, L.; Chen, Y. Synthesis of Anti-Pancreatic Cancer Natural Product Majusculamide D and Analogues Reveals a Preliminary Structure-Activity Relationships. *Chin. J. Chem.* **2024**, *42*, 605–610. [CrossRef]
49. Matos, Â.P.; Saldanha-Corrêa, F.M.P.; Gomes, R.D.S.; Hurtado, G.R. Exploring microalgal and cyanobacterial metabolites with antiprotozoal activity against Leishmania and Trypanosoma parasites. *Acta Trop.* **2024**, *251*, 107116. [CrossRef]
50. McPhail, K.L.; Correa, J.; Linington, R.G.; Gonzalez, J.; Ortega-Barría, E.; Capson, T.L.; Gerwick, W.H. Antimalarial linear lipopeptides from a Panamanian strain of the marine cyanobacterium *Lyngbya majuscula*. *J. Nat. Prod.* **2007**, *70*, 984–988. [CrossRef]
51. Shrestha, S.K.; Kim, S.W.; Soh, Y. Kalkitoxin attenuates calcification of vascular smooth muscle cells via RUNX-2 signaling pathways. *J. Vet. Sci.* **2023**, *24*, e69. [CrossRef] [PubMed]

52. Li, L.; Yang, M.; Shrestha, S.K.; Kim, H.; Gerwick, W.H.; Soh, Y. Kalkitoxin Reduces Osteoclast Formation and Resorption and Protects against Inflammatory Bone Loss. *Int. J. Mol. Sci.* **2021**, *22*, 2303. [CrossRef] [PubMed]
53. Huang, X.; Huang, W.; Li, L.; Sun, X.; Song, S.; Xu, Q.; Zhang, L.; Wei, B.G.; Deng, X. Structure Determinants of Lagunamide A for Anticancer Activity and Its Molecular Mechanism of Mitochondrial Apoptosis. *Mol. Pharm.* **2016**, *13*, 3756–3763. [CrossRef] [PubMed]
54. Hu, Y.; Mostert, D.; Orgler, C.; Andler, O.; Zischka, H.; Kazmaier, U.; Vollmar, A.M.; Braig, S.; Sieber, S.A.; Zahler, S. Thermal Proteome Profiling Reveals Insight to Antiproliferative and Pro-Apoptotic Effects of Lagunamide A in the Modulation of DNA Damage Repair. *Chembiochem* **2024**, *25*, e202400024. [CrossRef]
55. Luo, D.; Ratnayake, R.; Atanasova, K.R.; Paul, V.J.; Luesch, H. Targeted and functional genomics approaches to the mechanism of action of lagunamide D, a mitochondrial cytotoxin from marine cyanobacteria. *Biochem. Pharmacol.* **2023**, *213*, 115608. [CrossRef]
56. Huang, W.; Ren, R.G.; Dong, H.Q.; Wei, B.G.; Lin, G.Q. Diverse synthesis of marine cyclic depsipeptide lagunamide A and its analogues. *J. Org. Chem.* **2013**, *78*, 10747–10762. [CrossRef]
57. Zhao, L.; Thorsheim, C.L.; Suzuki, A.; Stalker, T.J.; Min, S.H.; Krishnaswamy, S.; Cockcroft, S.; Anderson, K.E.; Weiderhold, B.; Abrams, C.S. Individual phosphatidylinositol transfer proteins have distinct functions that do not involve lipid transfer activity. *Blood Adv.* **2023**, *7*, 4233–4246. [CrossRef]
58. Nile, A.H.; Tripathi, A.; Yuan, P.; Mousley, C.J.; Suresh, S.; Wallace, I.M.; Shah, S.D.; Pohlhaus, D.T.; Temple, B.; Nislow, C.; et al. PITPs as targets for selectively interfering with phosphoinositide signaling in cells. *Nat. Chem. Biol.* **2014**, *10*, 76–84. [CrossRef]
59. Decicco, C.P.; Grover, P. Total Asymmetric Synthesis of the Potent Immunosuppressive Marine Natural Product Microcolin A. *J. Org. Chem.* **1996**, *61*, 3534–3541. [CrossRef]
60. Andrus, M.B.; Li, W.; Keyes, R.F. Synthesis of Microcolin B, a Potent New Immunosuppressant Using an Efficient Mixed Imide Formation Reaction. *J. Org. Chem.* **1997**, *62*, 5542–5549. [CrossRef]
61. Mattern, R.H.; Gunasekera, S.; McConnell, O. Synthetic studies of microcolin B. *Tetrahedron* **1996**, *52*, 425–434. [CrossRef]
62. Mattern, R.H.; Gunasekera, S.P.; McConnell, O.J. Synthesis of microcolin analogs using trimethylsilylated lactamset. *Tetrahedron Lett.* **1997**, *38*, 2197–2200. [CrossRef]
63. Ye, Z.B.; Chen, J.; Meng, W.H.; Huang, P.Q. N-Benzyloxymalimide for an easy access to 5-alkyl-3-pyrrolin-2-ones: Asymmetric synthesis of the mixed imide substructure of the potent immunosuppressant microcolin B. *Tetrahedron Asymmetry* **2010**, *21*, 895–902. [CrossRef]
64. Vijayakumar, S.; Menakha, M. Tasiamide-B a new cyanobacterial compound for treating skin cancer. *Biomed. Prev. Nutr.* **2014**, *4*, 355–358. [CrossRef]
65. Robles-Bañuelos, B.; Durán-Riveroll, L.M.; Rangel-López, E.; Pérez-López, H.I.; González-Maya, L. Marine Cyanobacteria as Sources of Lead Anticancer Compounds: A Review of Families of Metabolites with Cytotoxic, Antiproliferative, and Antineoplastic Effects. *Molecules* **2022**, *27*, 4814. [CrossRef]